scientific reports

Check for updates

OPEN

Colorectal carcinoma progression is not influenced by the pseudokinase PEAK1

Alba Zuidema[1,2], Paul Atherton[1,3], Sabine van der Poel[1], Maaike Kreft[1], Ji-Ying Song[4], Martine Bierbooms[1], Sophie Verhoeven[1], Chrysoula Papagianni[1], Lona Kroese[5], Rahmen Bin Ali[5], Ivo Huijbers[5], Beatriz Carvalho[6] & Arnoud Sonnenberg[1]✉

The scaffold protein PEAK1 acts downstream of integrin adhesion complexes and the epidermal growth factor receptor, orchestrating signaling events that control cell proliferation and cytoskeletal remodeling. In this study we investigated the role of PEAK1 in colorectal carcinoma (CRC) progression using various in vitro and in vivo models to replicate the stepwise pathogenesis of CRC. While we observed a cell-type specific role for PEAK1 in the proliferation and in human CRC cell lines in vitro, our in vivo experiments using different CRC mouse models driven by loss of Apc, with or without oncogenic Kras or Pten loss suggest that PEAK1 does not significantly contribute to tumor formation in vivo. However, the survival time of *Peak1*$^{-/-}$ mice in the *Apc*$^{fl/+}$ model appeared to be slightly increased. Furthermore, PEAK1 promotes EGF-induced Caco-2 cell proliferation and regulates spheroid polarization and lumenization. Given that the Caco-2 cells harbor mutations in the tumor suppressors *APC* and *β-CATENIN*, but not in other tumor suppressors or in proto-oncogenes, we conclude that the PEAK1's impact on colon carcinogenesis is limited, potentially playing a role in the initial stage of the adenoma to carcinoma progression.

Keywords PEAK1, Colorectal carcinoma, KRAS, APC, PTEN, EGF

Colorectal cancer (CRC) is one of the most prevalent forms of cancer and the second most common cause of cancer-related deaths in the western world[1–3]. The disease begins with the formation of a benign adenoma, which can progress into an invasive cancer (carcinoma), eventually becoming metastatic. Common events in the multistep progression of CRC are mutational inactivation of tumor suppressor genes (*APC*, *PTEN*, *TP53*) and activation of oncogenes (*RAS*, *BRAF*, *PIK3CA*)[4–6]. Despite extensive knowledge of the genomic aberrations in CRC, it is still unclear how these affect the expression and activation status of proteins and signaling events that drive the adenoma-to-carcinoma progression. Because only 5% of the colorectal adenomas progress into carcinomas, there is a strong need to understand the biology of CRC development in order to predict which adenomas will progress and prevent patient over- or undertreatment[7].

The scaffold protein pseudopodium-enriched atypical kinase 1 (PEAK1) associates with integrin adhesion complexes and acts downstream of the epidermal growth factor receptor (EGFR) to coordinate signaling events that control cell proliferation, migration and cytoskeletal remodeling[8–10]. Integrins are cell adhesion receptors that are known to regulate a diverse array of cellular processes crucial to the formation and progression of solid tumors[11,12]. In addition, EGFR signaling is an important player in CRC initiation and progression[4]. As PEAK1 operates downstream of these receptor families, it is well placed to have a critical role in regulating the progression of colorectal adenoma to carcinoma.

Increased PEAK1 expression has been previously identified in multiple human malignancies, including breast, lung, and pancreatic cancer, contributing to disease progression[9,13–21]. On the other hand, elevated PEAK1 expression in gastric cancer, is correlated with improved patient survival[22]. In CRC, there is controversy

[1]Division of Cell Biology, The Netherlands Cancer Institute, Plesmanlaan 121, 1066 CX Amsterdam, The Netherlands. [2]Department of Oncological Urology and Laboratory Translational Oncology, Division of Imaging and Oncology, University Medical Center Utrecht, 3584 CX Utrecht, The Netherlands. [3]Department of Molecular and Clinical Cancer Medicine Institute of Systems, Molecular and Integrative Biology, The University of Liverpool, L69 7BE Liverpool, UK. [4]Experimental Animal Pathology, The Netherlands Cancer Institute, Amsterdam, Netherlands. [5]Mouse Clinic for Cancer and Aging research (MCCA) Transgenic Facility, The Netherlands Cancer Institute, Amsterdam, Netherlands. [6]Department of Pathology, The Netherlands Cancer Institute, Amsterdam, Netherlands. ✉email: a.sonnenberg@nki.nl

as to whether PEAK1 functions as a promoter or suppressor of tumor progression, as two studies on this subject reported contradicting findings[23,24].

In this study, we examined the role of PEAK1 in CRC disease progression by deleting PEAK1 in different in vitro and in vivo models in which lesions are combined that are frequently altered in CRC patients[4]. Our in vitro experiments using three human CRC cell lines indicate that PEAK1 promotes cell proliferation in response to EGF in Caco-2 cells, but not in SW480 or HT29 cells. PEAK1 also regulates cell polarity and lumenization of Caco-2 cells grown in 3D culture. However, our in vivo mouse experiments show that PEAK1 does not play a role in the formation of tumors driven by the loss of *Apc*, regardless of additional *Kras* activation or *Pten* loss.

Results

PEAK1 promotes Caco-2 cell proliferation upon EGF stimulation

Analysis of publicly available PEAK1 mRNA levels in colorectal carcinoma shows that high expression is associated with a worse prognosis (Fig. S1). To investigate the potential role of PEAK1 in CRC development, we first selected various microsatellite stable CRC cell lines harboring mutations in tumor suppressor and/or proto-oncogenes commonly found in CRC patients, to use as in vitro models. We selected Caco-2, SW480, and HT29 cells, all of which contain inactivating mutations in the *APC* gene. Additionally, the SW480 cell line harbors oncogenic mutations in the *KRAS* gene and HT29 in *BRAF* and *PIK3CA* genes[4,25,26] (Fig. 1a). We deleted PEAK1 in each of these cell lines using CRISPR/Cas9, obtaining two PEAK1 knockout clones using different guide RNAs targeting PEAK1 (Fig. 1b).

Next we compared the proliferation of PEAK1-deficient versus wild-type CRC cells (Fig. 1c, d,e). No significant differences in proliferation were observed between wild-type and PEAK1-deficient cells. Because PEAK1 plays a role in EGFR signaling[8], we explored whether PEAK1 exerts a regulatory effect on EGF-induced cell proliferation. To this end, we repeated the proliferation assays using EGF-supplemented cell culture medium and observed reduced proliferation of PEAK1-deficient Caco-2 cells compared to the wild-type cells (Fig. 1f). For SW480 cells we could observe a small decrease in proliferation of PEAK1-defecient cells for one of the two knockout cell lines (Fig. 1g). There was no significant difference in proliferation of HT29 wild-type versus PEAK1 knockout cells (Fig. 1h). It is important to note that EGF stimulation had no effect on the overall rate of proliferation of either the SW480 and HT29 cells; these cells have activating mutations in KRAS and BRAF, respectively, which may limit further activation of EGFR signaling.

Since loss of APC is an early step in adenoma formation, our results suggest that PEAK1 expression promotes cell proliferation in response to EGF stimulation at this stage. However, at later stages of adenoma to carcinoma progression, when other oncogenes have become activated, PEAK1 seems to play no role in regulating cell proliferation.

PEAK1 contributes to spheroid growth and lumen formation

Next, we investigated whether deletion of PEAK1 also affected cell growth in 3D by growing wild-type and PEAK1-deficient CRC cells as spheroids in Matrigel. For both Caco-2 and SW480 cells we observed a reduced size of PEAK1-deficient spheroids after growing the spheroids for 4–7 days in Matrigel (Fig. 2a, b). The HT29 spheroids (both wild-type and PEAK1-deficient) started to disintegrate after 4–7 days of culture in Matrigel and were not taken along in this analysis. To assess whether spheroid size could be used as a read-out for proliferation, we analyzed the number of cells and morphology of the spheroids by isolating spheroids on day 7 and staining the cell nuclei, cell-cell contacts, and actin cytoskeleton. While the SW480 spheroids were composed of a solid mass of cells, the Caco-2 spheroids formed a polarized cell layer surrounding a lumen (Fig. 2c), in line with previous studies[27,28]. Therefore, the reduced size observed for the PEAK1-deficient SW480 spheroids can be taken as an indication for a reduced proliferation of SW480 cells in 3D upon loss of PEAK1. However, Caco-2 spheroid size might not provide reliable information about the proliferative capacity of wild-type versus PEAK1 knockout cells in 3D due to the formation of the cyst-like structures, since the reduction in spheroid size could also be a result of impaired lumen formation.

To assess whether PEAK1 plays a role in the establishment of apical-basal polarity, we analyzed the ability of Caco-2 wild-type and PEAK1-deficient cells to form lumenized spheroids by isolating the spheroids after 7 days of culture in Matrigel and visualizing cell-cell contacts and the apical surface. We observed reduced lumen formation in PEAK1-deficient Caco-2 spheroids based on staining of PAR3, which forms an apical polarity complex with PAR6 and aPKC[29] (Fig. 2d, e). Next, we analyzed the expression of PAR3, E-cadherin, and the apical polarity protein Scribble[30,31] in the Caco-2 wild-type and knockout cells by western blot. Expression of Scribble, but not of PAR3 or E-cadherin, was reduced in both knockout cell lines (Fig. 2f). No obvious changes were observed in cell morphology and assembly of cell-cell junctions between wild-type and PEAK1-deficient Caco-2 cells seeded on coverslips (Fig. 2g), suggesting that the reduced lumen formation observed in the PEAK1-deficient Caco-2 spheroids is not caused by a defect in the organization of 2D adherens junctions.

In summary, PEAK1 regulates the size of Caco-2 cells cultured in Matrigel by regulating lumen formation.

Generation of a PEAK1-deficient mouse model

Due to the lack of physiologically relevant models to study the role of PEAK1 in development and tumorigenesis, we generated a *Peak1*$^{-/-}$ knockout mouse in the FVB/N background by pronuclear microinjection of CRISPR/Cas9 components. After at least 4 backcrosses of the *Peak1* knockout allele into the FVB/N strain, heterozygous *Peak*$^{+/-}$ mice were intercrossed to obtain homozygous *Peak1*$^{-/-}$ mice. The mice were monitored daily in the first weeks after birth and the role of PEAK1 in development was assessed by pathological analysis of mice homozygous for the deletion of PEAK1 (*Peak1*$^{-/-}$) shortly after birth and in 2-week-old, 2-month-old, or six-month-old animals (Fig. S2a). Deletion of PEAK1 was confirmed by PCR on genomic DNA (Fig. S2b). Wild-

a

	KRAS	*BRAF*	*PIK3CA*
Caco-2	wt	wt	wt
SW480	G12V	wt	wt
HT29	wt	V600E	P449T

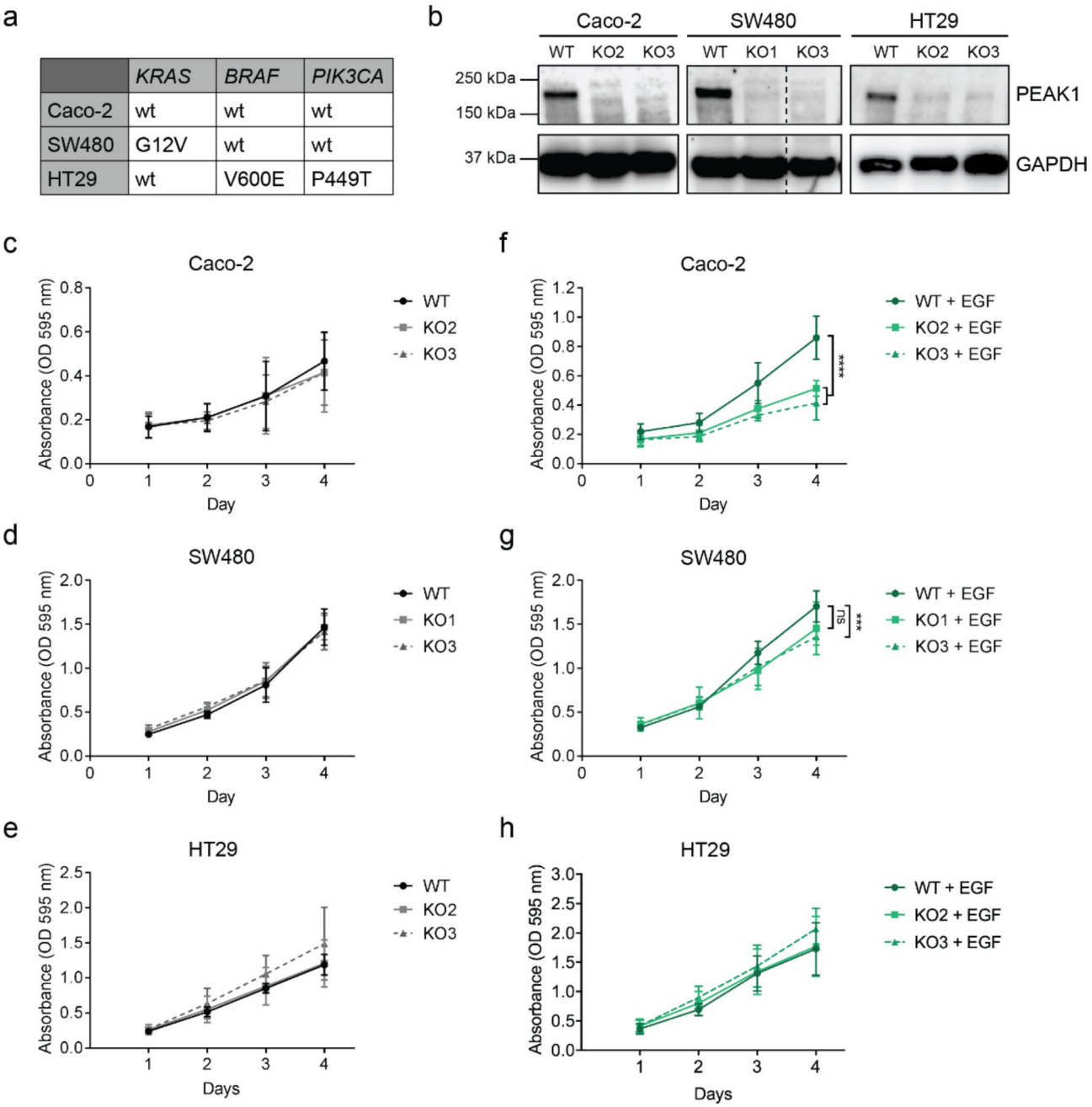

Fig. 1. PEAK1 promotes proliferation of Caco-2 cells stimulated with EGF. (**a**) Mutation status in CRC critical genes for the selected CRC cell lines. All cell lines contain mutations in *APC* and *TP53*. Adapted from Ahmed et al., [25] .**(b)** Western blots confirm deletion of PEAK1 in Caco-2, SW480, and HT29 cells that were transfected with CRISPR gRNAs 1–3. The number of the PEAK1 knockout (KO) indicates the gRNA used. GAPDH was used as loading control. Original blots are presented in Supplementary Fig. 4. **(c-g)** Proliferation assays were performed three times in triplicate. Cells were fixed on the indicated time points, stained with crystal violet, and absorbance was measured at 595 nm. Cell culture medium was either unsupplemented **(c-e)** or supplemented with 50 ng/ml EGF **(f-h)** at day 0. t-test was performed to determine statistical significance. ***, $P < 0.001$. ****, $P < 0.0001$. ns, not significant. Plots show mean with s.d.

type littermates were used as control in these experiments. Deletion of PEAK1 did not result in an abnormal phenotype during embryonic development, nor did it lead to pathological alterations in adult mice. At the time we started characterizing our *Peak1*$^{-/-}$ mice, another study was published that reported the generation of a *Peak1*$^{-/-}$ knockout mouse on a C57BL/6 background[32]. Similar to our findings, these mice did not reveal gross developmental or obvious health abnormalities, bred normally at expected Mendelian ratios, and had

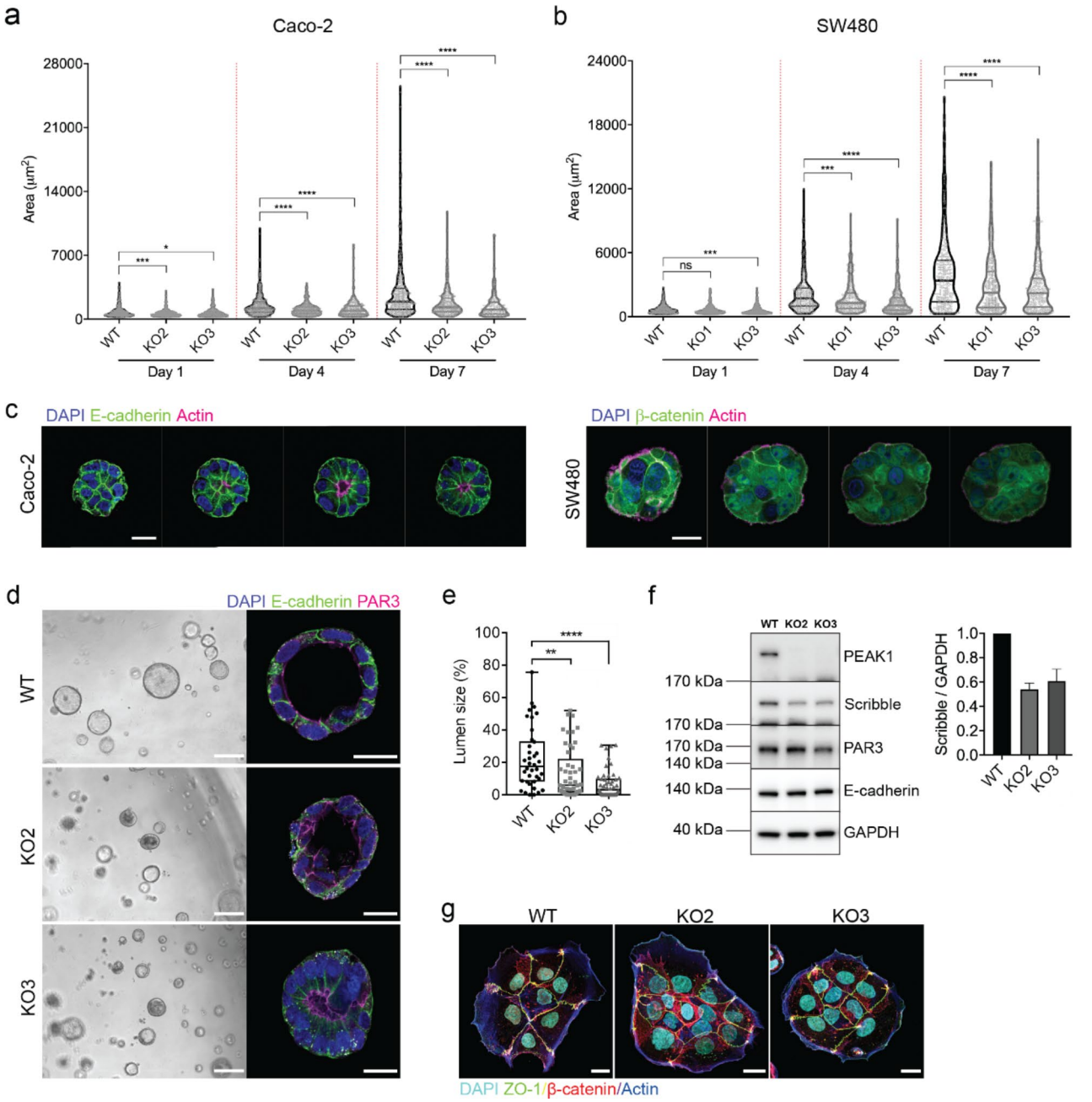

Fig. 2. Decreased size of PEAK1-deficient Caco-2 and SW480 spheroids. (**a,b**) Caco-2 **(a)** or SW480 **(b)** cells were seeded in Matrigel and imaged on day 1, 4 and 7. Data were obtained from three independent experiments. In total, 300–330 spheroids were analyzed per condition. **(c)** Confocal microscopy z-stack images of spheroids isolated from the Matrigel on day 7, showing E-cadherin (Caco-2) or β-catenin (SW480), actin, and the cell nuclei (stained with DAPI). Scale bar, 20 µm. **(d)** Caco-2 cells were seeded in Matrigel and imaged on day 7 using bright field microscopy (left panels). Scale bar, 200 µm. Subsequently, spheroids were isolated from the gels, stained for E-cadherin, PAR3, and the cell nuclei using DAPI, and imaged using confocal microscopy (right panels). Scale bar, 20 µm. **(e)** Quantifications of the lumen size as a percentage of the total spheroid size. Data were obtained from at least 3 independent experiments. Total number of spheroids analyzed: 38 (WT); 50 (KO2); 50 (KO3); 42 (WT + EGF); 38 (KO2 + EGF); 53 (KO3 + EGF). **(f)** Representative western blots showing the expression of Scribble, PAR3, and E-cadherin in PEAK1 wild-type and deficient Caco-2 cells. GAPDH was used as loading control. Quantifications of Scribble signal intensities normalized to GAPDH levels are shown ($n = 3$ for WT and KO2 samples; $n = 4$ for WT and KO3 samples; bars show mean with s.d.). Original blots are presented in Supplementary Fig. 4. (g) Immunofluorescence analysis of cell-cell junctions in Caco-2 cells seeded on coverslips and fixed after 3 days. Scale bar, 20 µm. Violin and box plots range from the smallest to largest value; lines indicate the median and 25th to 75th percentiles. Mann-Whitney U test was performed to determine statistical significance. *, $P < 0.05$; **, $P < 0.01$; ***, $P < 0.001$; ****, $P < 0.0001$.

normal complete blood counts. In this study it was shown that PEAK1 played an important role in regulating angiogenesis in the developing mouse retina[32].

As the mice aged, we observed a reduction in total body weight of the *Peak1*$^{-/-}$ mice compared to their wild-type littermates (Fig. S2c, d). These differences seemed mainly to be caused by changes in the weight of the white adipocyte tissue (Fig. S2e-g). Results of blood analysis showed that *Peak1*$^{-/-}$ mice have reduced levels of serum glucose, while cholesterol and triglyceride levels were not significantly altered (Fig. S3a). Similarly, total blood counts were not significantly changed (Fig. S3b). Since Wang et al.[32] did not report such defects, it is possible that strain-specific genetic factors may underlie the mild metabolic defect observed in our *Peak1* knockout mice.

PEAK1 does not play a role in CRC tumorigenesis in vivo

To determine whether PEAK1 can play a role in proliferation driven by activated Wnt signaling, we employed genetically engineered mouse models that either express or lack PEAK1 (*Peak1*$^{-/-}$) and in which a tamoxifen-inducible, intestinal epithelium-specific Cre-Recombinase (*VilCreER*^{T2}) excises floxed *Apc* alleles (*Apc*$^{fl/fl}$) to drive proliferation[33,34]. Intestinal hyperproliferation in the *VilCreER*^{T2}; *Apc*$^{fl/fl}$ and *VilCreER*^{T2}; *Apc*$^{fl/fl}$; *Peak1*$^{-/-}$ mice upon intraperitoneal (IP) injection of tamoxifen was compared by scoring proliferating cells in the small intestinal crypts based on BrdU staining (Fig. 3a-c). No significant differences were observed between the proliferating intestinal crypt cells of the two mouse strains.

Next, we examined the role of PEAK1 in CRC progression by using different CRC mouse models (*VilCreER*^{T2}; *Apc*$^{fl/+}$, *VilCreER*^{T2}; *Apc*$^{fl/+}$; *Kras*$^{G12D/+}$, and *VilCreER*^{T2}; *Apc*$^{fl/+}$; *Pten*$^{fl/fl}$) that develop spontaneous intestinal tumors upon induction with tamoxifen[33–35]. Overall, the results obtained using these three models show no significant differences in survival time and tumor burden in the small intestine between PEAK1 wild-type and deficient mice (Fig. 3d-o), although in the absence of PEAK1, the *VilCreER*^{T2}; *Apc*$^{fl/+}$ mice appeared to have a slightly increased survival time. Importantly, only 40% of the *VilCreER*^{T2}; *Apc*$^{fl/+}$ mice had to be sacrificed due to high tumor burden over the course of 1.5 year (Fig. 3e; Table S1). The other 60% of the mice either did not have any lesions (40%) or exhibited lesions that had not progressed into tumors (60%), based on histopathological analysis. Furthermore, no significant differences were observed between WT and *Peak1*$^{-/-}$ mice in histopathological analysis of the intestinal lesions from any of the three mouse models (Fig. 4). Taken together, these results indicate that PEAK1 most likely does not contribute to CRC progression in vivo.

Discussion

The scaffolding protein PEAK1 has been reported to regulate cellular signaling pathways that promote tumor growth and spread of cancer cells. The studies that focused on breast, lung, and pancreatic cancer reported supporting data for these functions of PEAK1[8,9,13–19,21,36–38]. In line with these findings, we previously described how PEAK1 interacts with tensin-3 to promote cell migration[10]. However, controversy exists about the role of PEAK1 in CRC, as it has been shown that PEAK1 can act both as a tumor promotor and a suppressor[23,24].

In this study we aimed to unravel the role of PEAK1 in CRC progression. Initially, we examined the effect of PEAK1 deletion on cell growth in vitro using a panel of microsatellite stable human cell lines: Caco-2 (an adenoma-like cell type) and SW480 and HT29 cells (carcinoma-like cell types). Cell proliferation was reduced in both PEAK1-deficient Caco-2 cell lines upon treatment with EGF, while this effect on proliferation was only minor in SW480 cells and not present in HT29 cells. This may be due to the fact that, in contrast to the Caco-2 cells, SW480 and HT29 cells harbor oncogenic mutations in the *KRAS* and *BRAF/PIK3CA* genes, respectively. As PEAK1 can directly bind to the adaptor proteins Shc1 and Grb2, it is believed to act downstream of the EGFR but upstream of KRAS and BRAF[8,10,39]. Therefore, the deletion of PEAK1 in the SW480 and HT29 cells might not have a major effect on signaling events downstream of the EGFR that regulate cell proliferation. In contrast to the 2D proliferation assays, PEAK1-deficient SW480 spheroids show reduced growth compared to wild-type spheroids. The proliferation differences observed in 2D versus 3D can be attributed to distinct activation of signaling events[40,41]. However, PEAK1 does not contribute to tumor incidence and growth in the *VilCreER*^{T2}; *Apc*$^{fl/+}$; *Kras*$^{G12D/+}$ CRC mouse model and thus does not play a major role in oncogenic Kras-driven CRC progression.

To study the role of PEAK1 in spontaneous CRC development, we crossed *Peak1*$^{-/-}$ mice with different CRC mouse models. The results of the *VilCreER*^{T2}; *Apc*$^{fl/+}$, *VilCreER*^{T2}; *Apc*$^{fl/+}$; *Kras*$^{G12D/+}$, and *VilCreER*^{T2}; *Apc*$^{fl/+}$; *Pten*$^{fl/fl}$ mouse tumor models indicate that PEAK1 does not play a role in tumorigenesis, when comparing the survival time and tumor burden between PEAK1 wild-type and deficient mice. A limitation of these mouse models is that the mice have to be sacrificed due to the high tumor burden before the onset of invasion and metastasis[42,43]. In particular, the *VilCreER*^{T2}; *Apc*$^{fl/+}$ mice exhibited a slower-than-expected rate of tumor development, with only about 40% of the mice developing tumors after 1.5 years. PEAK1 might play a minor role in early tumor formation, as indicated by a slight (though not statistically significant, potentially due to the low n numbers) increase in survival of the *Peak1*$^{-/-}$ mice in this model. This would be in line with our findings that PEAK1 deletion hampers Caco-2 growth in response to EGF and in 3D culture (Figs. 1 and 2).

To address whether PEAK1 regulates metastatic spreading one could employ orthotopic organoid transplantations, in which case intestinal crypt cells are isolated from the different mouse strains, cultured as organoids in vitro, and transplanted into the colon or cecal epithelium[44,45]. While the genetically engineered mouse models used in this study are more physiologically relevant for investigating CRC progression compared to subcutaneous injection of cell lines into nude mice[23,24], a further limitation is that the tumors predominantly form in the small intestine rather than the colon[42,43].

Given that inbred mouse strains with Apc mutations show varying susceptibilities to tumor development[46], we cannot exclude the possibility that the absence of an observed effect of PEAK1 on CRC could be attributed to genetic background. However, the results from our mouse models (mixed FVB/N; C57BL/6J background)

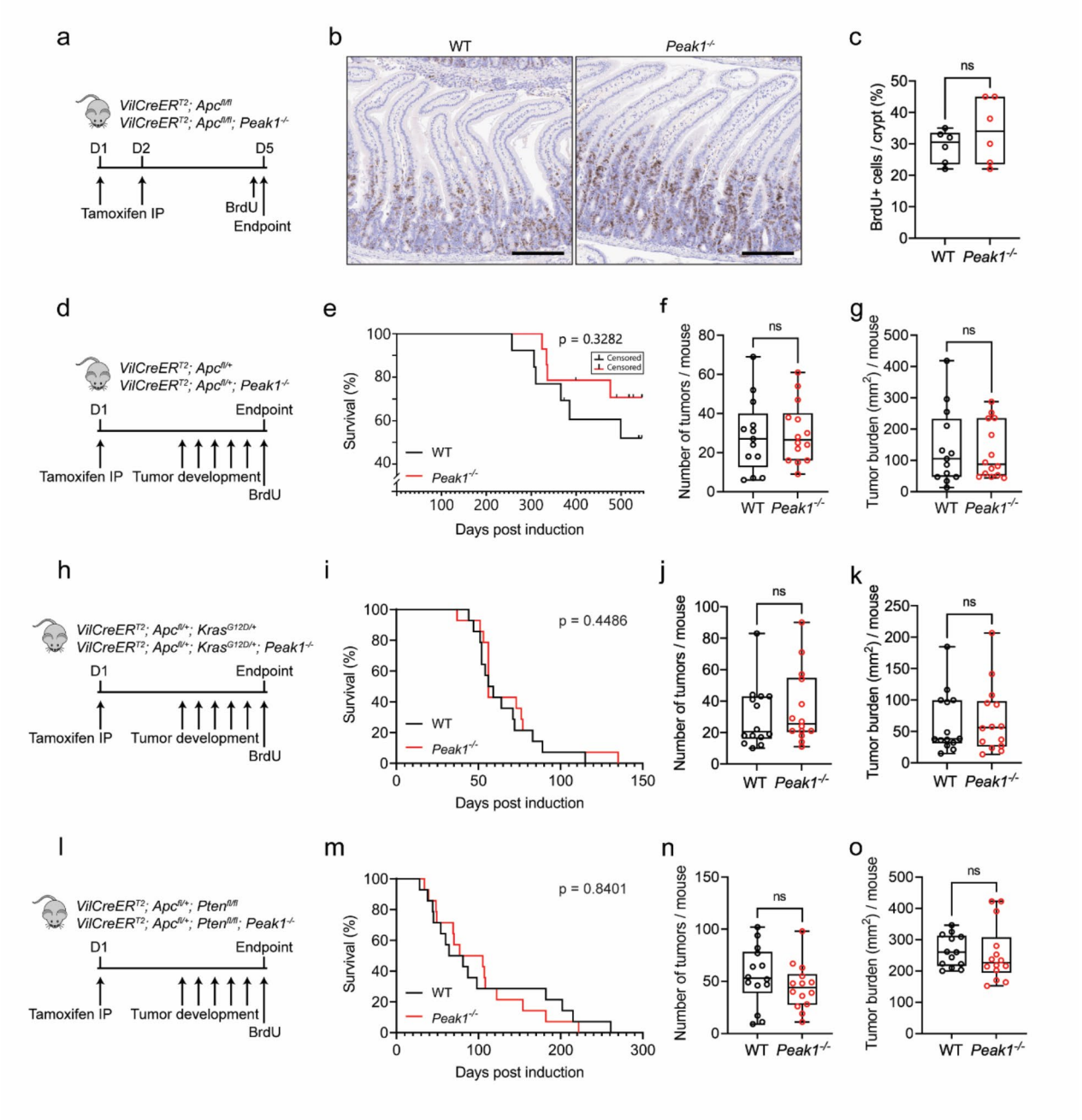

Fig. 3. PEAK1 does not promote CRC progression in vivo. **(a)** Timeline of the short-term *VilCreER*^{T2}; *Apc*$^{fl/fl}$ mouse models to study hyperproliferation. **(b)** BrdU incorporation in the small intestine of *VilCreER*^{T2}; *Apc*$^{fl/fl}$ (WT) and *VilCreER*^{T2}; *Apc*$^{fl/fl}$; *Peak1*$^{-/-}$ (*Peak1*$^{-/-}$) mice, visualized by immunohistochemistry. Scale bar, 200 µm. **(c)**. The average percentages of BrdU-positive cells per crypt are shown. Each point represents the average percentage per mouse ($n = 6$ mice per group; at least 25 crypts per sample were scored). **(d**, **h**, **l)** Timeline of the long-term mouse models to study tumorigenesis. Mice were injected with tamoxifen and sacrificed when they showed symptoms of intestinal tumors (Endpoint). **(e**, **i**, **m)** Kaplan-Meier survival plots comparing WT versus *Peak1*$^{-/-}$ mice after Cre-Recombinase induction with tamoxifen. Around day 540 all remaining *VilCreER*^{T2}; *Apc*$^{fl/+}$ (WT) and *VilCreER*^{T2}; *Apc*$^{fl/+}$; *Peak1*$^{-/-}$ (*Peak1*$^{-/-}$) animals were sacrificed. Censored animals are indicated on the Kaplan-Meier curve as tick marks. Survival data and information for censoring are provided in Supplementary Table S1. **(e)**. P values were calculated using the log-rank (Mantel-Cox) test **(f**, **j**, **n)**. The number of tumors in the small intestine was scored macroscopically at the endpoint of the experiment. **(g**, **k**, **o)**. The tumor burden was defined as the sum of the area (πr^2) of all tumors. $n = 14$ mice per group, except for *VilCreER*^{T2}; *Apc*$^{fl/+}$ (WT) and *VilCreER*^{T2}; *Apc*$^{fl/+}$; *Pten*$^{fl/fl}$ (WT) $n = 13$. Mann-Whitney U test was performed to determine statistical significance. ns, not significant.

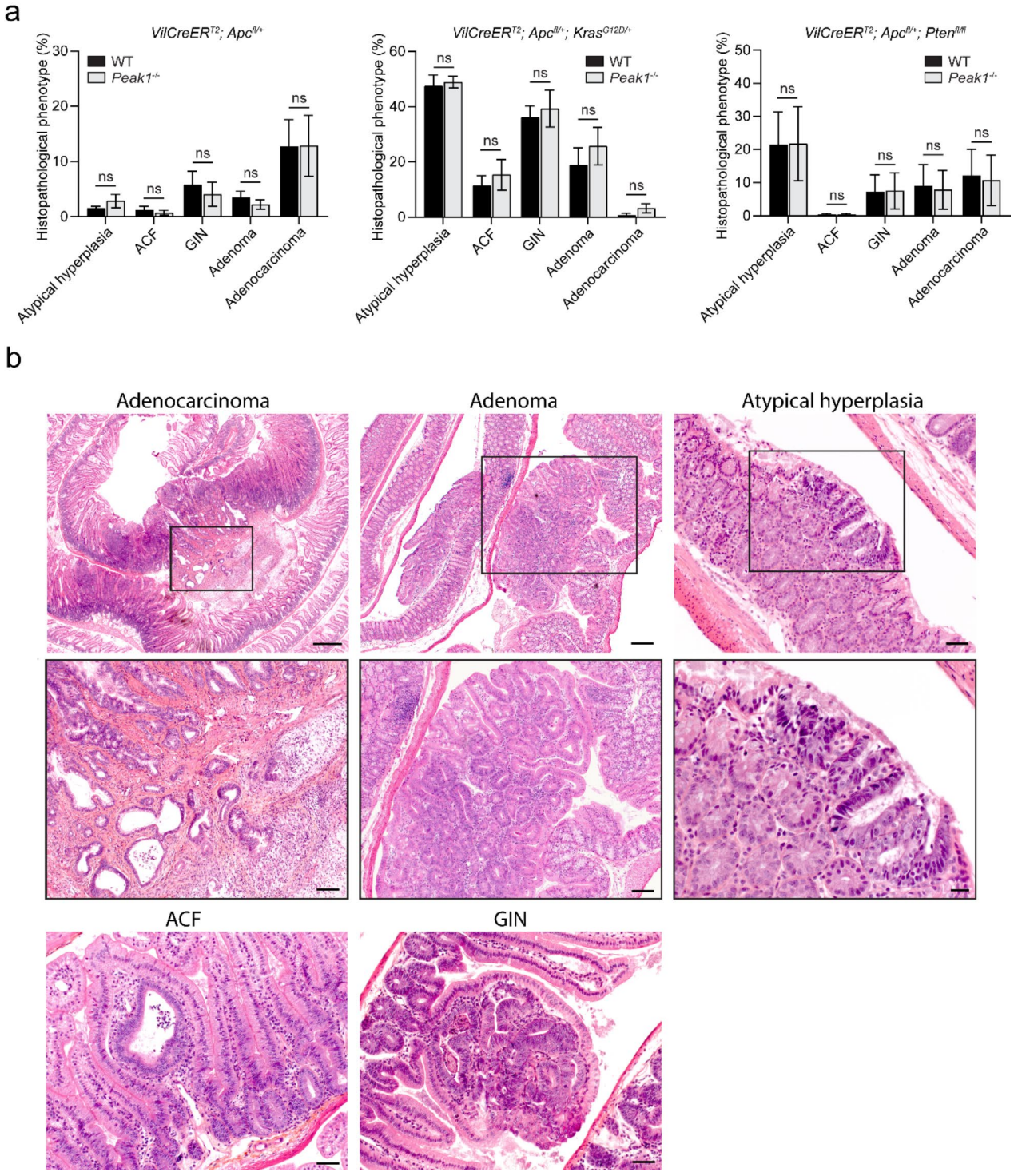

Fig. 4. Pathological analysis of intestinal lesions.The entire intestinal tract, including duodenum/jejunum, ilium, cecum, proximal colon, and distal colon/rectum,was examined in both WT and *Peak1*$^{-/-}$ mice for specific lesions, such as aberrant crypt foci (ACF), gastrointestinal intraepithelial neoplasia (GIN), adenoma, and adenocarcinoma. (**a**) Histograms illustrate the percentage of each lesion type present in the intestines of mice with different genotypes. Lesions were scored as detailed in the Materials and Methods section. Error bars represent the standard error of the mean; ns denotes not significant (Two-Way ANOVA with Šídák's multiple comparison test between groups); For each group, $n = 5$, representing the 5 sections of the GI tract that were analyzed. (**b**) Microphotographs of H&E-stained sections illustrate each type of lesion as described. Scale bars: Upper panel: 500 µm (left), 200 µm (middle), 50 µm (right.). Middle panel: 100 µm (left and middle), 20 µm (right). Lower panel: 50 µm (left and right).

align with the survival probability described by Davies et al.[35], when examining adenoma development ($Apc^{fl/+}$) in outbred mice.

In summary, we investigated the role of PEAK1 in the colorectal adenoma-to-carcinoma progression by deleting PEAK1 in both human in vitro and mouse in vivo CRC models. Our results indicate that in vivo PEAK1 is not involved in the regulation of intestinal cell proliferation driven by activated Wnt signaling due to loss of APC nor in promoting tumorigenesis driven by oncogenic Kras and/or loss of Apc/Pten. However, PEAK1 does promote Caco-2 in vitro cell proliferation upon EGF stimulation and 3D spheroid polarization and lumenization. The obtained results indicate that PEAK1 could be involved in the regulation of colorectal cancer cell proliferation and polarity, but only in a context-dependent manner and during the early stages of tumorigenesis. Based on our mainly negative in vivo and in vitro data, we conclude that PEAK1 does not drive the colorectal adenoma-to-carcinoma progression.

Materials and methods

Antibodies

Primary antibodies used are listed in Table 1. Secondary antibodies were as follows: goat anti-rabbit Alexa Fluor 488, goat anti-mouse Alexa Fluor 568, goat anti-rabbit or anti-mouse Alexa Fluor 647 (Invitrogen), stabilized goat anti-mouse or anti-rabbit HRP-conjugated (Bio-Rad) and rabbit anti-goat HRP-conjugated (Zymax).

Cell lines

Caco-2, HT29, and SW480 cell lines were cultured in Dulbecco's modified Eagle's medium (DMEM) containing 10% heat-inactivated fetal bovine serum (FBS) and antibiotics and maintained at 37 °C in a humidified, 5% CO_2 atmosphere. Authentication of the cell lines was done by testing 16 DNA markers by short tandem repeat analysis (Eurofins Genomics, Ebersberg, Germany).

Generation of PEAK1-deficient cells

The target gRNAs against human *PEAK1* (exon4; 5'-GTGGGCTTCACAGCTATAGT-3', 5'-TGTGAAGCC CACTATGATAG-3', and 5'-TGCCCGTGTTCCTGATGCGG-3', referred to as gRNA1, gRNA2, and gRNA3, respectively) were cloned into pX330-U6-Chimeric_BB-CBh-hSpCas9 (a kind gift from Feng Zhang[47]; Addgene plasmid #42230). Cells were transfected with this vector using lipofectamine® 2000 (Invitrogen) and selected with 2.5 μg ml^{-1} puromycin for 3 days following transfection.

Western blotting

Cells were washed in cold PBS, lysed in RIPA buffer (20 mM Tris-HCl, pH 7.5, 100 mM NaCl, 4 mM EDTA, 1% Nonidet P-40, 0.1% SDS, 0.5% sodium deoxycholate) supplemented with a protease inhibitor cocktail (Sigma), 1.5 mM Na_3VO_4, and 15 mM NaF, and cleared by centrifugation at 14.000 x *g* for 30 min at 4 °C. Lysates were mixed with sample buffer (50 mM Tris-HCl, pH 6.8, 2% SDS, 10% glycerol, 12.5 mM EDTA, 0.02% bromophenol blue) containing a final concentration of 2% β-mercaptoethanol and denatured at 95 °C for 5 min. Proteins were separated by electrophoresis using Bolt Novex 4–12% gradient Bis-Tris (Invitrogen) or homemade 6% polyacrylamide gels, transferred to Immobilon-P transfer membranes (Millipore Corp) and blocked for at least 30 min in 2% BSA in TBST buffer (10 mM Tris, pH 7.5, 150 mM NaCl, and 0.2% Tween-20). Primary antibody (diluted in 2% BSA in TBST buffer) incubation took place overnight at 4 °C. After washing twice with TBST and twice with TBS buffer, blots were incubated for 1 h hour at room temperature with horseradish peroxidase–conjugated secondary antibodies (diluted 1:3.000 in 2% BSA in TBST buffer). After subsequent washing steps, the bound antibodies were detected by enhanced chemiluminescence using Clarity™ Western ECL Substrate (Bio-Rad) as described by the manufacturer. Signal intensities were quantified using ImageJ[48,49].

Proliferation assays

Cells were seeded in 96-well plate (SW480 and HT29: 10.000 cells/well; Caco-2: 7,500 cells/well) in triplicate. Cells were fixed after 1, 2, 3, or 4 days with 2% paraformaldehyde for 10 min, gently washed 3 times with H_2O and air-dried. Fixed cells were stained with 100 μl of 5 mg/ml crystal violet (dissolved in 2% ethanol) at room temperature on a plate shaker for 10 min, rinsed three times with H_2O and then air- dried. Subsequently, the

Antibody	Clone	Obtained from	Host	Application
PEAK1	D4G6J	Cell Signaling Technology (#72908)	Rabbit	IF: 1:100 WB: 1:1000
GAPDH	6C5	EMD Millipore (#CB1001)	Mouse	WB: 1:5000
β-catenin		BD Trans. (#610154)	Mouse	IF: 1:100
BrdU		Dako (#M 0744)	Mouse	IHC: 1:100
E-cadherin	36	BD Biosciences	Mouse	IF: 1:100 WB: 1:2000
PAR3	H-70	Santa Cruz (#sc-98509)	Rabbit	IF: 1:50 WB: 1:500
Scribble	C-20	Santa Cruz (#sc-11048)	Goat	WB: 1:500
ZO-1		Zymed (#61-7300)	Rabbit	IF: 1:100

Table 1. Primary antibody list.

DNA-bound crystal violet was solubilized with 100 µl of 2% SDS in H_2O and its absorbance was measured at 595 nm on a microplate reader (Bio-Rad) using MPM5 software.

Spheroids

Cells (5×10^3 cells/well) were mixed with 2% Matrigel in culture medium and seeded in a 96-wells plate coated with Matrigel (70 µl/well). Images were taken 1, 4 and 7 days after seeding, using a Zeiss Axiovert 200 M microscope with an A-Plan 10×/0.25 Ph1 M27 objective. Spheroids were isolated after 7 days, by incubating the gels with 100 µl recovery solution (Corning) for 1 h at 4 °C. The spheroid-containing gels were resuspended and transferred to an Eppendorf tube, washed three times with cold PBS and cleared by centrifugation at 1200 rpm for 3 min at 4 °C, spheroid suspensions were placed in a square drawn with Dako (hydrophobic) pen on poly-L-lysine (0.1% w/v in H_2O; ChemCruz)-coated slides and fixed with 4% paraformaldehyde for 10 min. Image analysis was performed using Fiji (ImageJ)[48,49].

Immunofluorescence

Subconfluent cells were fixed with 2% paraformaldehyde for 10 min, permeabilized with 0.2% Triton-X-100 for 5 min, and blocked with PBS containing 2% BSA (Sigma) for at least 30 min. Next, cells were incubated with the primary antibodies for 1 h at room temperature (for 2D experiments) or overnight at 4 °C (for spheroids). Cells were washed three times before incubation with the secondary antibodies for 1 h. Additionally, the nuclei were stained with DAPI and filamentous actin was visualized using Alexa Fluor 488 or 647-conjugated phalloidin (Biolegend; AAT Bioquest). After three washing steps with PBS, the coverslips were mounted onto glass slides in Mowiol. Images were obtained at room temperature using a Leica TCS SP5 confocal microscope with a AOBS scan head (158001107; Leica), controlled using Leica LAS AF SP5 software (v2.7.4), with a with a 63x (NA 1.4) oil objective (2D experiments) or 63x (NA 1.2) water objective (spheroids), with filter cubes for 488/eGFP (15525302; Leica), 568/mCherry (15525303; Leica), and DAPI (15525301; Leica).

Animal experiments

All animal studies were undertaken in accordance with the Dutch guidelines for care and use of laboratory animals and were approved by the Central Authority for Scientific Procedures on Animals (CCD), license number AVD3010020172464.

Findings and experiments described in this paper were designed and reported following the Animal Research: Reporting of In Vivo Experiments (ARRIVE) guidelines. For tumor growth studies, mice were allowed to age until they showed clinical signs of intestinal disease (anaemia, hunched back and/or weight loss). Mice were euthanized using carbon dioxide (CO_2).

The (conditional) PEAK1 knockout mice were generated using CRISPR/Cas9 genome editing by pronuclear microinjection of 50 ng/µl in vitro transcribed Cas9 mRNA, 25 ng/µl gRNAs targeting the *Peak1* intronic regions flanking exons 4–7 (5'-GGGATTGATTTTTAGCGCACTGG-3' and 5'-TGCTATATGAGTAGCCACTCTGG-3') and two single-stranded oligodeoxynucleotides repair templates containing the *loxP* site (5'-ATAACTTCG TATAGCATACATTATACGAAGTTAT-3') flanked by 60 bp homology arms (Integrated DNA Technologies). After backcrossing to the FVB/N background, mice were obtained with a floxed *Peak1* allele ($Peak1^{+/fl}$) and complete deletion ($Peak1^{+/-}$). After at least 4 backcrosses to FVB/N background, the heterozygous $Peak^{+/-}$ mice were intercrossed to obtain homozygous $Peak1^{-/-}$ mice. The genotypes were analyzed by PCR on genomic DNA using the following primers: P1: 5'-CCCGGGTTTGCCTTTGATAC-3', P2: 5'-GCCTGGCGATGGCAAGAAT A-3', and P3: 5'-CCATCTCCTCTAGCTGACCCTT-3'. In one PCR reaction, primers P1 and P2 were combined to detect a WT band (218 bp) and P2 and P3 were combined to detect a KO band (189 bp).

No embryonic lethality or pathological alterations related to the genotype were observed in $Peak1^{-/-}$ mice. These mice were intercrossed with $VilCreER^{T2}$; $Apc^{fl/fl}$; $Kras^{G12D/+}$ or *VilCreERT2;* $Apc^{fl/+}$; $Pten^{fl/+}$ (kindly provided by William Faller) to obtain the strains described in the figures.

The animals were kept in a pathogen-free, temperature-controlled environment with a 12 h dark / 12 h light cycle. Mice received standard chow and acidified water *ad libitum*. Roughly equal numbers of male and female animals were used. Male and female mice were housed separately, and 2–5 mice were housed per cage. Mice used for experiments were of mixed FVB/N - C57BL/6J background.

Sample size calculations were performed using two-sample t test, powered to detect a mean difference of 30% at a power of 0.85 to a p-value of 0.05 assuming a 25% group standard deviation using a Java Applet for Power and Sample Size (Lenth, R. V. (2006-9). Retrieved March 2020, from http://www.stat.uiowa.edu/~rlenth/Power). For short-term studies to analyze hyperproliferation of the intestinal epithelium, 6 animals per group were used. For long-term studies of spontaneous tumor development, 14 animals per group were used.

All animals were injected intraperitoneally with 80 mg/kg of tamoxifen dissolved in sunflower oil on day 1 to induce Cre-Lox recombination. For tumor studies, animals were monitored 2–3 times a week until they showed signs of tumor formation, which included weight loss, hunching, paling feet from anaemia, and/or development of a prolapse. Animals were injected intraperitoneally with 50 mg/kg BrdU 2 h before dissection. Tumors were scored macroscopically by counting the numbers of visible tumors after fixation of the opened intestinal tissue in ethanol glacial acetic acid mixture (3:1), containing 2% of formaldehyde (EAF).

For short-term experiments, animals were injected with a second dose of tamoxifen on day 2 and BrdU on day 5, 2 h before dissection. Intestinal tissues were fixed in EAF, embedded in paraffin, and BrdU was visualized by immunohistochemistry. Images were taking on an Aperio ScanScope, using ImageScope software version 12.0.0 (Aperio). No randomization was used. Researchers were blinded to genotypes during the macroscopical tumor scoring and counting of the BrdU-positive cells per crypt.

Histopathological analysis of intestinal lesions

Entire intestinal tract was collected and segmented in duodenum, jejunum, ileum, cecum, proximal colon, distal colon, and rectum/anus. They were fixed in EAF fixative (ethanol: acetic acid: formaldehyde: saline at 40:5:10:45 v: v) and embedded in paraffin blocks, from which sections of 2 µm thickness were made and stained with hematoxylin and eosin (HE) according to standard procedures. Microphotographs were made with a Zeiss AxioCam HRc digital camera and processed with AxioVision 4 software (both from Carl ZeissVision, München, Germany). Histopathological analysis was conducted blindly by an experienced laboratory animal pathologist. Lesions were classified as atypical hyperplasia, aberrant crypts, GIN (gastrointestinal intraepithelial neoplasia), adenoma, and adenocarcinoma as described in[46]. The number of each type of lesions in each segment of the intestine was counted and the intensity of each type of lesions was summarized as mild + (1–5 lesions), moderate ++ (5–10 lesions), and severe +++ (more than 10 lesions). Furthermore, organs such as spleen, liver, lung, and/or stomach etc. were also collected along with for an observation of possible metastasis.

The percentage of each lesion phenotype present for wild type and *Peak1*$^{-/-}$ mouse models was calculated by first multiplying the number of each lesion type by either 0, 0.25, 0.5, or 1 for -, +, ++, or +++, respectively to generate a ranked scoring. The sum of the ranked scoring was divided by the total number of lesions for each segment of the GI tract and multiplied by 100.

Analysis of PEAK in colon cancer

Kaplan-Meier curves were generated using mRNA levels from gene chip data using kmplot.com[50], searching for PEAK1 (Affymetrix ID: 225913_at). Analysis was performed across all subtypes with no restrictions to any cohorts.

Statistical analysis

Mann-Whitney U or t-test (two-tailed P value) and log-rank (Mantel-Cox) test were performed using GraphPad Prism (version 9). In figures, statistically significant values are shown as $*P<0.05$; $**P<0.01$; $***P<0.001$; $****P<0.0001$. Graphs were made in GraphPad Prism and show all data points.

Data availability

All data generated during this study are included in the article and its supplementary files or are available from the corresponding author on reasonable request.

Received: 8 April 2024; Accepted: 4 November 2024
Published online: 12 November 2024

References

1. Siegel, R. L. et al. Colorectal cancer statistics, 2020. *CA Cancer J. Clin.* **70** (3), 145–164 (2020).
2. Siegel, R. L., Miller, K. D. & Jemal, A. Cancer statistics, 2020. *CA Cancer J. Clin.* **70** (1), 7–30 (2020).
3. Ferlay, J. et al. Cancer incidence and mortality patterns in Europe: estimates for 40 countries and 25 major cancers in 2018. *Eur. J. Cancer*. **103**, 356–387 (2018).
4. Markowitz, S. D. & Bertagnolli, M. M. Molecular origins of cancer: molecular basis of colorectal cancer. *N Engl. J. Med.* **361** (25), 2449–2460 (2009).
5. Vogelstein, B. et al. Genetic alterations during colorectal-tumor development. *N Engl. J. Med.* **319** (9), 525–532 (1988).
6. Fearon, E. R. & Vogelstein, B. A genetic model for colorectal tumorigenesis. *Cell.* **61** (5), 759–767 (1990).
7. Sillars-Hardebol, A. H. et al. The adenoma hunt in colorectal cancer screening: defining the target. *J. Pathol.* **226** (1), 1–6 (2012).
8. Zheng, Y. et al. Temporal regulation of EGF signalling networks by the scaffold protein Shc1. *Nature*. **499** (7457), 166–171 (2013).
9. Wang, Y. et al. Pseudopodium-enriched atypical kinase 1 regulates the cytoskeleton and cancer progression [corrected]. *Proc. Natl. Acad. Sci. U S A*. **107** (24), 10920–10925 (2010).
10. Zuidema, A. et al. PEAK1 Y635 phosphorylation regulates cell migration through association with Tensin3 and integrins. *J. Cell. Biol.*, **221** (8). e202108027 (2022).
11. Desgrosellier, J. S. & Cheresh, D. A. Integrins in cancer: biological implications and therapeutic opportunities. *Nat. Rev. Cancer*. **10** (1), 9–22 (2010).
12. Hamidi, H. & Ivaska, J. Every step of the way: integrins in cancer progression and metastasis. *Nat. Rev. Cancer*. **18** (9), 533–548 (2018).
13. Ding, C. et al. Overexpression of PEAK1 contributes to epithelial-mesenchymal transition and tumor metastasis in lung cancer through modulating ERK1/2 and JAK2 signaling. *Cell. Death Dis.* **9** (8), 802 (2018).
14. Kelber, J. A. et al. KRas induces a Src/PEAK1/ErbB2 kinase amplification loop that drives metastatic growth and therapy resistance in pancreatic cancer. *Cancer Res.* **72** (10), 2554–2564 (2012).
15. Fujimura, K. et al. A hypusine-eIF5A-PEAK1 switch regulates the pathogenesis of pancreatic cancer. *Cancer Res.* **74** (22), 6671–6681 (2014).
16. Strnadel, J. et al. eIF5A-PEAK1 signaling regulates YAP1/TAZ protein expression and pancreatic Cancer cell growth. *Cancer Res.* **77** (8), 1997–2007 (2017).
17. Croucher, D. R. et al. Involvement of Lyn and the atypical kinase SgK269/PEAK1 in a basal breast cancer signaling pathway. *Cancer Res.* **73** (6), 1969–1980 (2013).
18. Agajanian, M. et al. PEAK1 acts as a Molecular switch to regulate context-dependent TGFbeta responses in breast Cancer. *PLoS One*. **10** (8), e0135748 (2015).
19. Abu-Thuraia, A. et al. AXL confers cell migration and invasion by hijacking a PEAK1-regulated focal adhesion protein network. *Nat. Commun.* **11** (1), 3586 (2020).
20. Runa, F., Adamian, Y. & Kelber, J. A. Ascending the PEAK1 toward targeting TGF during cancer progression: Recent advances and future perspecctives. *Cancer Cell. Microenviron*, **3** (1), e1162 (2016).
21. Hamalian, S. et al. A SNAI2-PEAK1-INHBA stromal axis drives progression and lapatinib resistance in HER2-positive breast cancer by supporting subpopulations of tumor cells positive for anti-apoptotic and stress signaling markers. *Oncogene*, **40**(33), 5224–5235 (2021).
22. Guo, Q. et al. Analysis of a cytoskeleton-associated kinase PEAK1 and E-cadherin in gastric cancer. *Pathol. Res. Pract.* **210** (12), 793–798 (2014).

23. Ding, C. et al. The PEAK1-PPP1R12B axis inhibits tumor growth and metastasis by regulating Grb2/PI3K/Akt signalling in colorectal cancer. *Cancer Lett.* **442**, 383–395 (2019).
24. Huang, L. et al. PEAK1, acting as a tumor promoter in colorectal cancer, is regulated by the EGFR/KRas signaling axis and miR-181d. *Cell. Death Dis.* **9** (3), 271 (2018).
25. Ahmed, D. et al. Epigenetic and genetic features of 24 colon cancer cell lines. *Oncogenesis*. **2**, e71 (2013).
26. Berg, K. C. G. et al. Multi-omics of 34 colorectal cancer cell lines - a resource for biomedical studies. *Mol. Cancer*. **16** (1), 116 (2017).
27. Jaffe, A. B. et al. Cdc42 controls spindle orientation to position the apical surface during epithelial morphogenesis. *J. Cell. Biol.* **183** (4), 625–633 (2008).
28. Magudia, K., Lahoz, A. & Hall, A. K-Ras and B-Raf oncogenes inhibit colon epithelial polarity establishment through up-regulation of c-myc. *J. Cell. Biol.* **198** (2), 185–194 (2012).
29. Ohno, S. Intercellular junctions and cellular polarity: the PAR-aPKC complex, a conserved core cassette playing fundamental roles in cell polarity. *Curr. Opin. Cell. Biol.* **13** (5), 641–648 (2001).
30. Assemat, E. et al. Polarity complex proteins. *Biochim. Biophys. Acta*. **1778** (3), 614–630 (2008).
31. Bonello, T. T. & Peifer, M. Scribble: a master scaffold in polarity, adhesion, synaptogenesis, and proliferation. *J. Cell. Biol.* **218** (3), 742–756 (2019).
32. Wang, H. et al. Pseudopodium-enriched atypical kinase 1 mediates angiogenesis by modulating GATA2-dependent VEGFR2 transcription. *Cell. Discov.* **4**, 26 (2018).
33. Knight, J. R. P. et al. MNK Inhibition sensitizes KRAS-Mutant Colorectal Cancer to mTORC1 inhibition by reducing eIF4E phosphorylation and c-MYC expression. *Cancer Discov.* **11** (5), 1228–1247 (2021).
34. Shibata, H. et al. Rapid colorectal adenoma formation initiated by conditional targeting of the apc gene. *Science*. **278** (5335), 120–123 (1997).
35. Davies, E. J. et al. PTEN loss and KRAS activation leads to the formation of serrated adenomas and metastatic carcinoma in the mouse intestine. *J. Pathol.* **233** (1), 27–38 (2014).
36. Liu, L. et al. Homo- and Heterotypic Association regulates signaling by the SgK269/PEAK1 and SgK223 pseudokinases. *J. Biol. Chem.* **291** (41), 21571–21583 (2016).
37. Pan, M., Yin, X. & Huang, Y. C. Pseudopodium enriched atypical kinase 1(PEAK1) promotes invasion and of melanoma cells by activating JAK/STAT3 signals. *Bioengineered*. **12** (1), 5045–5055 (2021).
38. Fujimura, K. et al. KRAS Oncoprotein expression is regulated by a self-governing eIF5A-PEAK1 feed-Forward Regulatory Loop. *Cancer Res.* **78** (6), 1444–1456 (2018).
39. Krasinskas, A. M. EGFR Signaling in Colorectal Carcinoma. *Patholog Res. Int.* **2011**, 932932 (2011).
40. Riedl, A. et al. Comparison of cancer cells in 2D vs 3D culture reveals differences in AKT-mTOR-S6K signaling and drug responses. *J. Cell. Sci.* **130** (1), 203–218 (2017).
41. Pickl, M. & Ries, C. H. Comparison of 3D and 2D tumor models reveals enhanced HER2 activation in 3D associated with an increased response to trastuzumab. *Oncogene*. **28** (3), 461–468 (2009).
42. McIntyre, R. E. et al. Mouse models of colorectal cancer as preclinical models. *Bioessays*. **37** (8), 909–920 (2015).
43. Burtin, F., Mullins, C. S. & Linnebacher, M. Mouse models of colorectal cancer: past, present and future perspectives. *World J. Gastroenterol.* **26** (13), 1394–1426 (2020).
44. Fumagalli, A. et al. A surgical orthotopic organoid transplantation approach in mice to visualize and study colorectal cancer progression. *Nat. Protoc.* **13** (2), 235–247 (2018).
45. Roper, J. et al. Colonoscopy-based colorectal cancer modeling in mice with CRISPR-Cas9 genome editing and organoid transplantation. *Nat. Protoc.* **13** (2), 217–234 (2018).
46. Boivin, G. P. et al. Pathology of mouse models of intestinal cancer: consensus report and recommendations. *Gastroenterology*. **124** (3), 762–777 (2003).
47. Cong, L. et al. Multiplex genome engineering using CRISPR/Cas systems. *Science*. **339** (6121), 819–823 (2013).
48. Schindelin, J. et al. Fiji: an open-source platform for biological-image analysis. *Nat. Methods*. **9** (7), 676–682 (2012).
49. Schneider, C. A., Rasband, W. S. & Eliceiri, K. W. NIH Image to ImageJ: 25 years of image analysis. *Nat. Methods*. **9** (7), 671–675 (2012).
50. Kovacs, S. A., Fekete, J. T. & Gyorffy, B. Predictive biomarkers of immunotherapy response with pharmacological applications in solid tumors. *Acta Pharmacol. Sin.* **44** (9), 1879–1889 (2023).

Acknowledgements

We would like to thank William Faller and Rob van der Kammen for providing mouse strains and assistance with the animal experiments and the NKI Animal and BioImaging facilities for support.

Author contributions

A. Zuidema: Conceptualization, visualization, writing (original draft; review & editing), formal analysis, investigation, data curation, supervision. S. v.d. Poel: Investigation, data curation. M. Kreft: Investigation, data curation. P. Atherton: Writing (original draft; review & editing), visualization, supervision, formal analysis. JY. Song: Formal analysis. M. Bierbooms: Investigation. S. Verhoeven: Investigation. C. Papagianni: Investigation. L. Kroese: Resources. R. Bin Ali: Resources. I. Huijbers: Resources. B. Carvalho: Resources. A. Sonnenberg: Conceptualization, funding acquisition, supervision, project administration, writing (review & editing).

Declarations

Competing interests

The authors declare no competing interests.

Additional information

Supplementary Information The online version contains supplementary material available at https://doi.org/10.1038/s41598-024-78776-7.

Correspondence and requests for materials should be addressed to A.S.